Arch. Metall. Mater. **68** (2023), 3, 851-860

DOI: https://doi.org/10.24425/amm.2023.145447

M. MIRMEHDI[1], A. BOOCHANI[2*], S.R. MASHARIAN[1]

ELECTRONIC, OPTICAL AND TRANSPORT PROPERTIES OF HfNiSn UNDER MN IMPURITY

In this work, the electronic structure and optical behavior and the thermoelectric performance of the known HfNiSn compound have been studied under the substitution of Mn transition metal instead of Ni atoms. Necessary calculations are performed in the framework of DFT first principles studies by applying generalized gradient approximation (PBE-GGA) as well as solving Boltzmann's semi-classical equations. The entering Mn leads to a change in the electronic structure of HfNiSn and the occurrence of half-metallic ferromagnetic behavior with 100% polarization at the Fermi level. The maximum ZT value obtained for HfMnSn shows that HfNiSn would be suitable for thermoelectric applications at room temperature, both in pure and Mn presence. The examination of optical parameters also indicates good absorption in the visible range for this compound in all cases.

Keywords: HfNiSn; Half-metallic; Optical property; Transport

1. Introduction

The well-known Heusler group, including transition metals based on MNiSn (M = Ti, Hf, Zr), has been extensively studied, and they have demonstrated semiconductor behavior with the good thermoelectric performance [1-5]. These Heusler compounds with MgAgAs-type structure and 18 valence electrons have attracted a lot of attention in recent years due to their high thermo-power and suitable electronic conductivity [6-10]. In this structure with F4-3m space group, M atoms have been localized in (0.0.0), Ni in (0.25.0.25.0.2.25) and Sn in (0.75.0.75.0.75). The thermoelectric performance of these materials can be described by measuring the dimensionless figure of merit $ZT = (S^2\sigma T)/K$, which T is temperature, S is Seebeck coefficient, σ is electrical conductivity, and k is the amount of thermal conductivity including the electron and lattice contributions ($K = K_{el} + K_{latt}$). Investigation of the electronic structure of these compounds, including the band structure and the density of states, indicates the non-magnetic semiconductor behavior due to a narrow and indirect bandgap in the vicinity of the two points of C and X [11,12]. The highest value of ZT among the half-Heusler structures of MM'NiSn (M, M' = Hf, Ti, Zr) belongs to the $Zr_{0.5}Hf_{0.5}NiSn$ alloy, which is about 0.5 at 700K [13-15]. However, the challenge in studying these materials is still the high lattice thermal conductivity, which is a significant obstacle in the path of thermoelectric applications. One of the best ways to reduce lattice conduction is to dope the composition with transition metals to increase the lattice phonon scattering, and consequently, the conduction will drop significantly. Many theoretical and experimental studies have been done. The results of Sb substitution instead of Sn in this half-Heusler can be mentioned, which leads to a decrease in the lattice thermal conductivity to about 5-6 W/mK to reach a ZT about 0.7 at 800K [15-20]. In 2005, Sakurada and Shutoh showed that at about 700K, the Zr0.25Hf0.25Ti0.5NiSn0.99 Sb0.002 alloy receives the highest ZT about 1.5 [14], or doping Zr0.5Hf0.5NiSn with Pd are other results in this field to achieve the Zr0.5Hf0.5Ni0.8Pd0.2Sn0.99Sb0.01 compound with the figure of merit about 0.6 [7].

In the following work, the crystalline structure and stability of HfNiSn are first examined using DFT calculations under the substitution of manganese atoms instead of Ni atoms in the half-Heusler phase. In the next step, the electronic structure, including the band structure and states' density, are investigated. It continues by examining the optical parameters, including dielectric function, electron loss spectra, absorption, reflection, and refraction coefficients. Finally, the thermoelectric behavior of this doped half-Heusler is discussed.

1 DEPARTMENT OF PHYSICS, HAMEDAN BRANCH, ISLAMIC AZAD UNIVERSITY, HAMEDAN, IRAN
2 DEPARTMENT OF PHYSICS, KERMANSHAH BRANCH, ISLAMIC AZAD UNIVERSITY, KERMANSHAH, IRAN

* Corresponding author: arash_bch@yahoo.com

© 2023. The Author(s). This is an open-access article distributed under the terms of the Creative Commons Attribution-NonCommercial License (CC BY-NC 4.0, https://creativecommons.org/licenses/by-nc/4.0/deed.en which permits the use, redistribution of the material in any medium or format, transforming and building upon the material, provided that the article is properly cited, the use is noncommercial, and no modifications or adaptations are made.

2. Computational details

Calculations of the electronic structure and the optical parameters are performed within the DFT framework by Wien2K code [21-23]. Solving the Kohn-Sham equation governing the problem have been done using the full potential augmented plane wave plus local orbitals (FP-LAPW+lo) method for the valence and core electrons. The generalized gradient approximation (GGA) has been applied in the form of Perdew-Burke-Ernzerhof for exchange-correlation energy [24]. The computational values are considered as $R_{mt}K_{max} = 8.5$, the radius of the Muffin-Tin spheres for Hf = 2.30au, Ni = 2.10au, Sn = 2.20au, and 2000 K points for the first Brillouin zone meshing with 14×14×14 in Monkhorst-pack design [25]. Also, the G_{max} and l_{max} are 13.5, and 10, respectively. Effects of manganese substitution in the HfNiSn combination with FCC cube structure, F-43m space group and atomic Wyckoff positions for Hf, Ni and Sn, respectively: 4a (0.0.0), 4c (0.25, 0.25, 0.25) and 4b (0.5, 0.5.0.5) with experimental lattice constant of 6.11A [12,26]. Besides, this compound's electron transport behavior under substitution is studied using the semi-classical BoltzTraP code [27].

3. Results and discussion

3.1. Structural properties

As mentioned in Section 2, the half-Heusler HfNiSn, and HfMnSn compounds have an FCC structure with three Hf, Ni(Mn), and Sn atoms on each base. To construct the structure of these compounds in the Wi2n2K software with the F-43m space group, either their primitive cell or their conventional cell can be built (see Fig. 1). It is clear that in the FCC structure, the conventional cell is four times larger than its primitive cell. There are **twelve** atoms in the above-mentioned conventional cell, four Hf atoms, four Ni(Mn) atoms, and four Sn atoms.

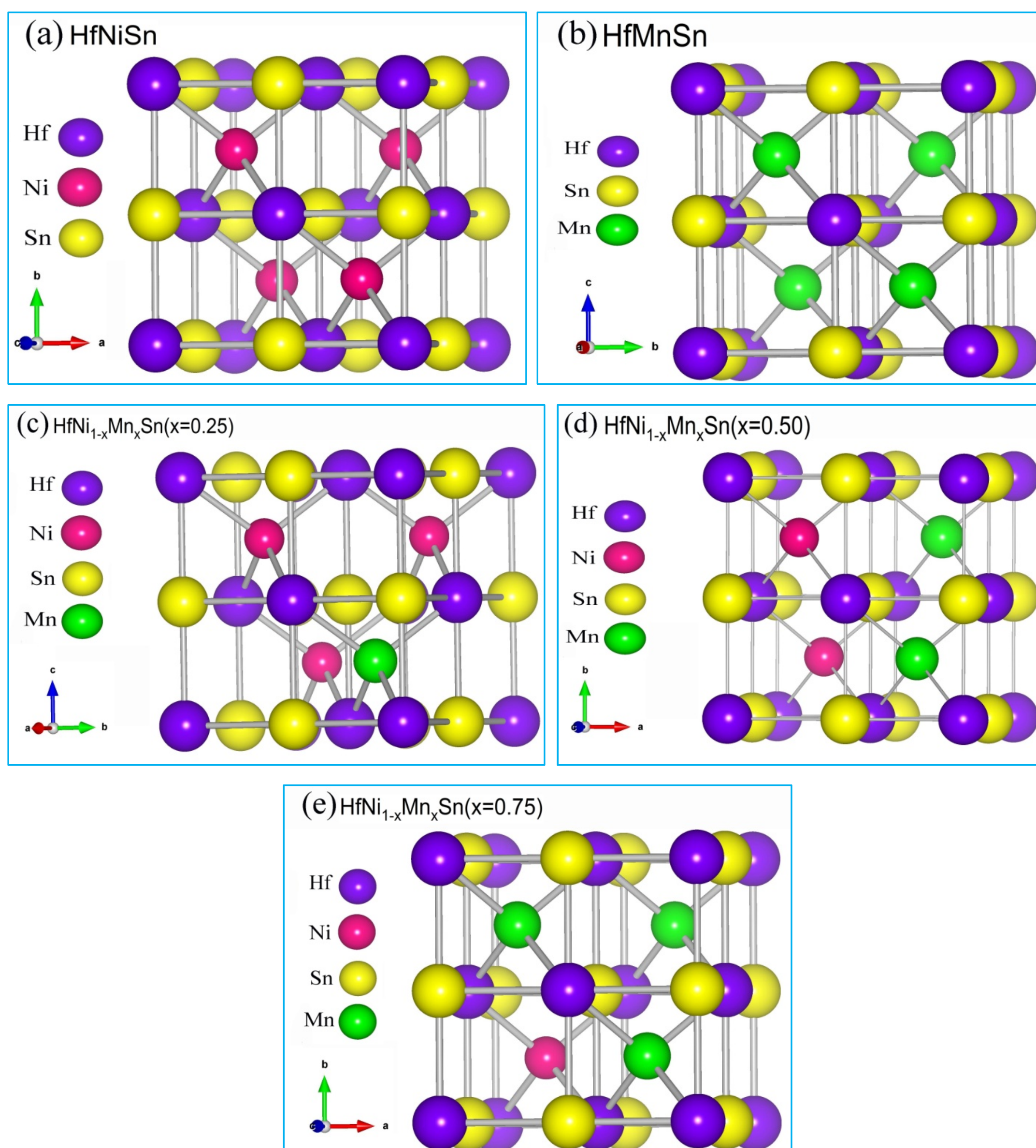

Fig. 1. The convectional cell of the $HfNi_{1-x}Mn_xSn$ (x = 0, 0.25, 0.5, 0.75, 1) compounds

Therefore, to achieve the mentioned percentages of substitution, we have substituted one to four Mn atoms for Ni atoms. To making $HfNi_{1-x}Mn_xSn$ (x = 0, 0.25, 0.5, 0.75, 1) compounds with the presence of Mn substitutions because the symmetry of the crystal changes, we have used a conventional cell.

It should be noted that the space groups of $HfNi_{1-x}Mn_xSn$ compounds for x = 25%, 50%, and 75% are P-43m, P-4m2, and P-43m, respectively, which have 24, 8, 24 symmetric matrices, while in pure combination with the F-43m space group, there have 24 symmetric matrices. The presence of Mn atoms in the HfNiSn structure has increased the crystalline anisotropy, shown in the symmetric matrices of their space group and the shape of the energy-volume curves. It is shown that in x = 50% substitution case occurred lower crystal isotropic.

In the first step, the total energy variations of the crystal in terms of the unit cell volume are calculated by fitting the data based on the Birch Murnaghan equation [28], as shown in Fig. 2. Lattice equilibrium parameters, including lattice constant, bulk modulus (B), the derivative of bulk modulus (B') and formation energy (E_f) in thermodynamic equilibrium, are presented in TABLE 1 for pure and doped structures with different percentages. It is noteworthy that the calculations are considered for both spin channels. It can be seen that the HfNiSn lattice constant is well consistent with other reports [12] and it increases with the rise in the percentage of the manganese substitution. It is shown that the total energy of ground state of HfMnSn is lower than HfNiSn compound.

All these curves have a minimum point, so they all have an equilibrium volume where the crystal is in equilibrium. The diagrams of HfNiSn and HfMnSn compounds are perfectly symmetric, indicating their high crystalline symmetry and that under stress and strain, we see symmetrical mechanical responses from them. But in the other four energy-volume diagrams, it can be seen that the slope of their curves is steeper in smaller volumes than the slope in larger volumes, which indicates that they are more resistant to stress.

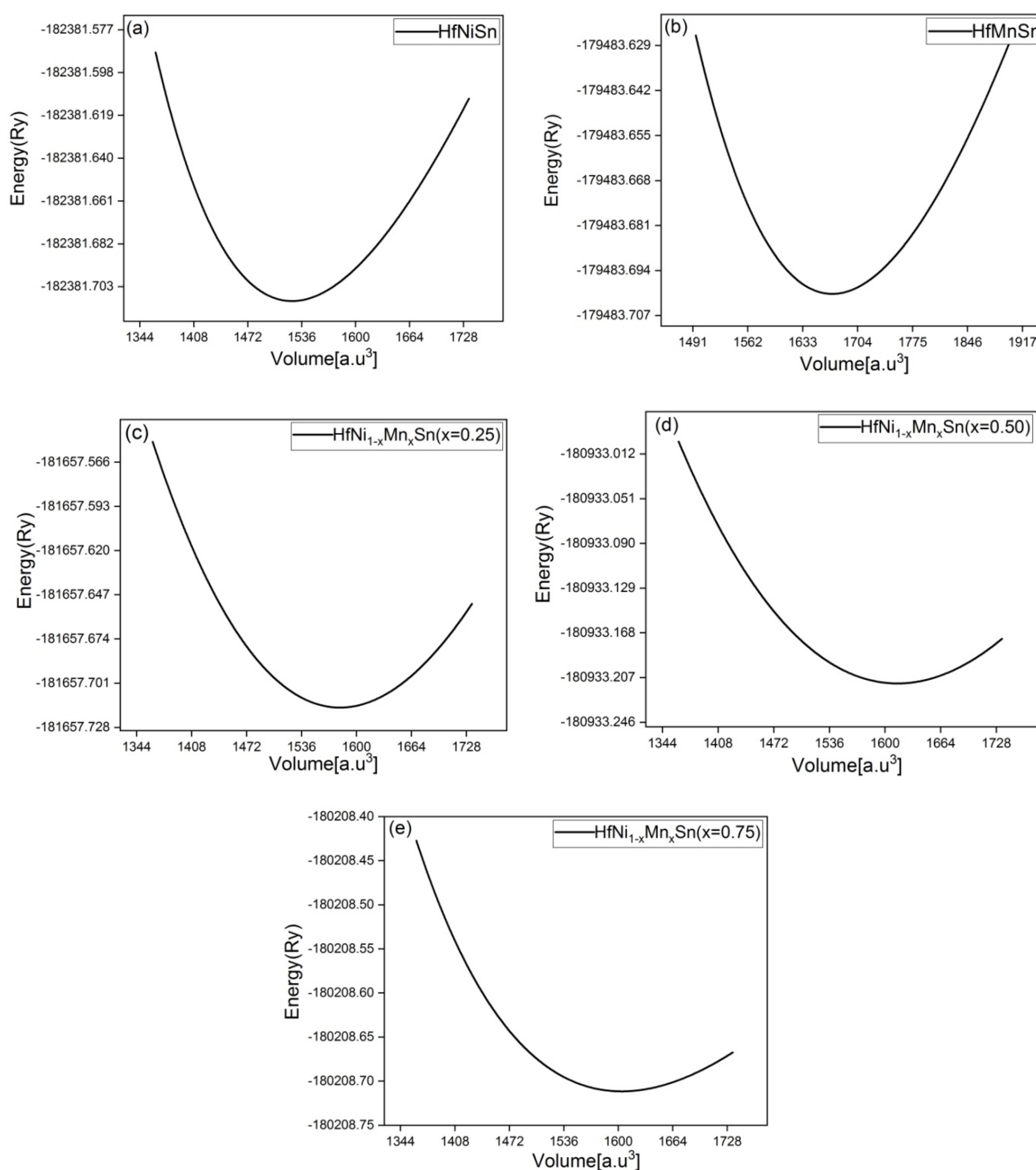

Fig. 2. The Energy-Volume (E-V) curves of the (a) HfNiSn, (b) $HfNi_{0.75}Mn_{0.25}Sn$, (c) $HfNi_{0.5}Mn_{0.5}Sn$, (d) $HfNi_{0.25}Mn_{0.75}Sn$, and (e) HfMnSn in the ferro-magnetic phase

TABLE1

The lattice parameters (a), bulk modulu (B) and its pressure derivative (B'), band gap (eV), formation energy (E_f), and total energy of equilibrium point (E_{tot}) for Mn-substituated HfNiSn compound

Parametr	a(^{0}A)	B (Gpa)	B'	E_g(eV)	E_f(Ry)	E_{tot}(Ry)
HfNiSn	6.091	147.95	7.784	0.24	–0.226	–45595.6251
HfMnSn	6.280	91.03	5.641	0.50	–0.229	–44871.1251
$HfNi_{1-x}Mn_xSn$(x = 0.25)	6.164	137.10	1.982	0.49	–0.181	–181657.7148
$HfNi_{1-x}Mn_xSn$(x = 0.50)	6.207	136.46	1.669	0.46	–0.180	–180933.2152
$HfNi_{1-x}Mn_xSn$(x = 0.75)	6.260	97.58	5.787	0.48	–0.180	–180208.7173

3.2. Electronic properties

In this section, the electronic properties and characteristics of HfNiSn have been examined under substituted. The total density of states (TDOS) curves are shown in Fig. 3(a to e). According to the results, the HfNiSn compound is a non-magnetic semiconductor; however, it is observed that with increasing Mn substitution instead of Ni, the rate of magnetism and spin

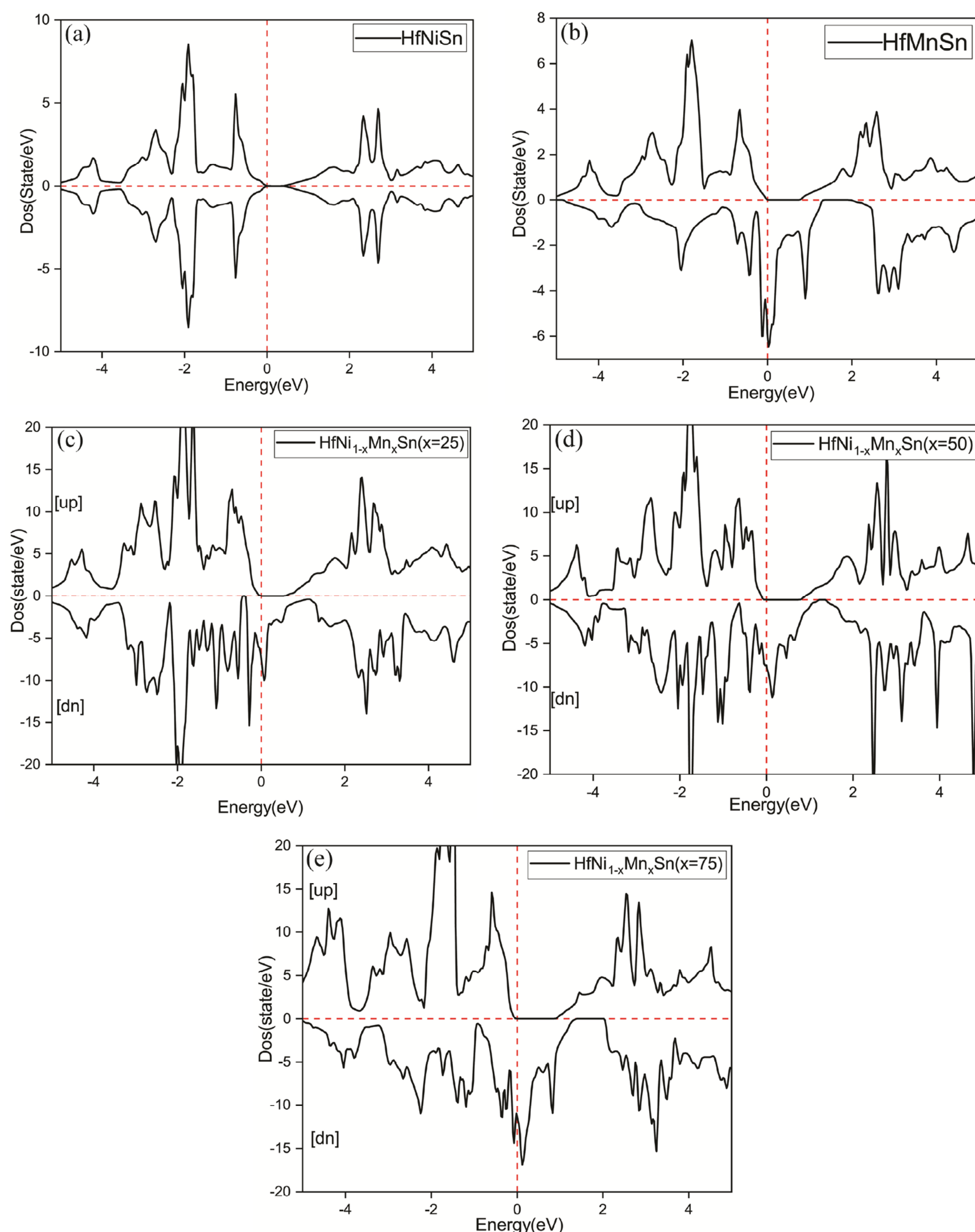

Fig. 3. TDOS of the (a) HfNiSn, (b) HfMnSn, (c) $HfNi_{0.5}Mn_{0.5}Sn$, (d) $HfNi_{0.25}Mn_{0.75}Sn$, and (e) $HfN_{i0.25}Mn_{0.75}Sn$., for tow up and down spins by GGA

polarization increases at the Fermi level. In all of these alloys, semiconductor behavior in spin up and metallic behavior in spin down can be observed, which indicates the occurrence of half-metallic ferromagnetic behavior due to the presence of Mn. It is worth mentioning that two alloys of HfNi0.75Mn0.25Sn and HfNi0.5Mn0.5Sn are electrically unstable, especially in the Spin down, the DOS curves are jagged. It is important to note that in spin up, there is a more balanced form of DOS in all percentages of substitution, especially HfNi0.25Mn0.75Sn and HfMnSn. With the appearance of the Van Hove singularities in the compounds, the energy gap converts to spin-flip. The values of these gaps are given in TABLE 1.

For a better comparison, we repeated the TDOS curves in Fig. 4 with the mBJ approximation, for up and down spins. It can be seen that in this figure no noticeable change in electronic properties is observed and somehow the GGA approximation results are repeated.

The band structure diagrams also show n-type semiconductor behavior for HfNiSn with narrow indirect gaps about 0.24eV of Fig. 5, which is in perfect agreement with DOS curves, similar to other results [12,29]. As can be seen in the band structure in Fig. 5, the maximum valence band of this compound is at point Γ, and its minimum conduction band is at point X. For all pure and doped states, the valence bands' intertwining is evident in the range of –4eV to the Fermi level. In contrast, the conduction levels have higher gradients, which means the electrons' increased mobility in these compounds. It is also observed that a gap separates the core and semi-core regions from the valence region.

Several important events have occurred by entering the Mn substitutions: firstly, the compound has become a magnetic

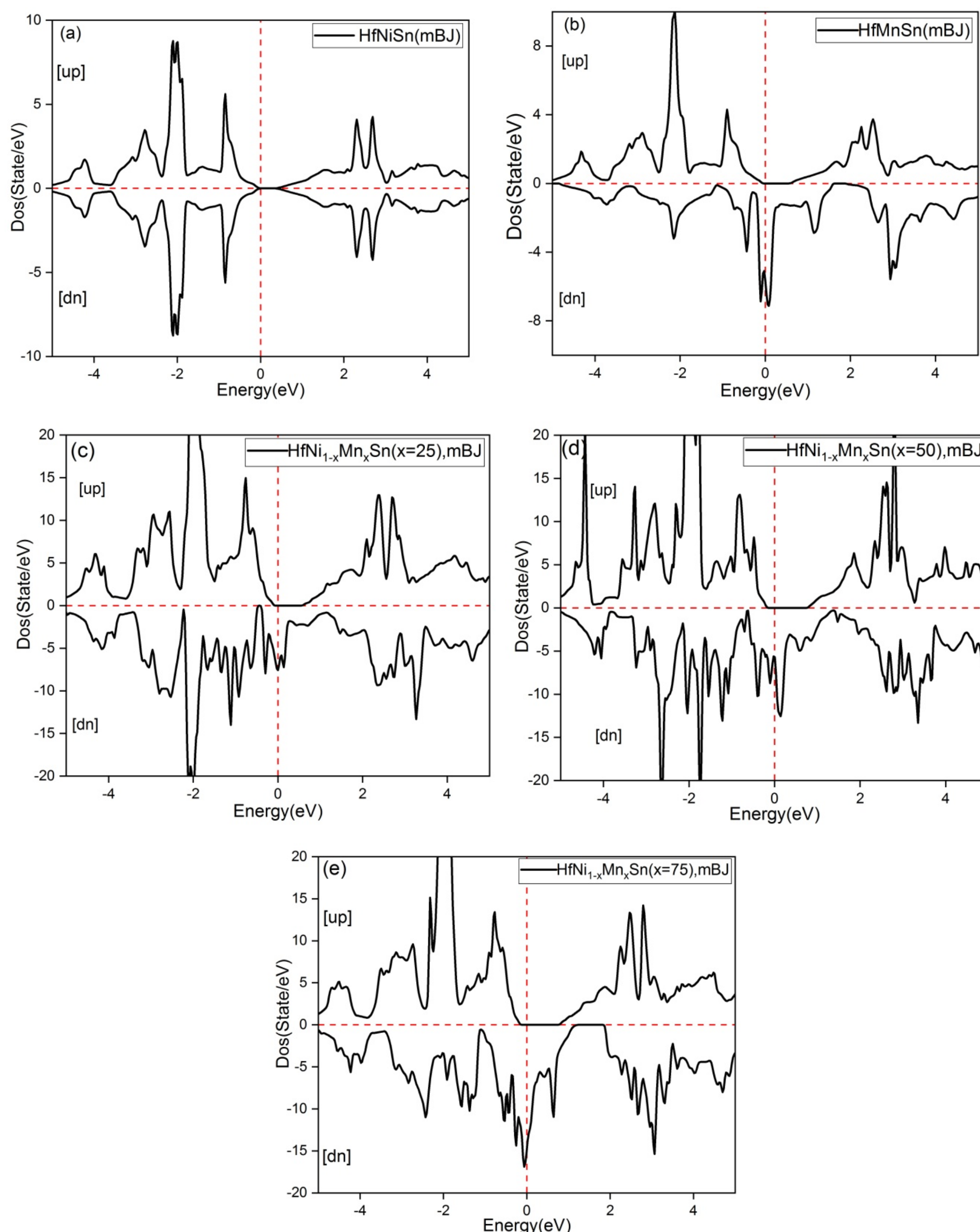

Fig. 4. TDOS of the (a) HfNiSn, (b) HfMnSn, (c) $HfNi_{0.5}Mn_{0.5}Sn$, (d) $HfNi_{0.25}Mn_{0.75}Sn$, and (e) $HfN_{i0.25}Mn_{0.75}Sn$., for tow up and down spins by mBJ approximation

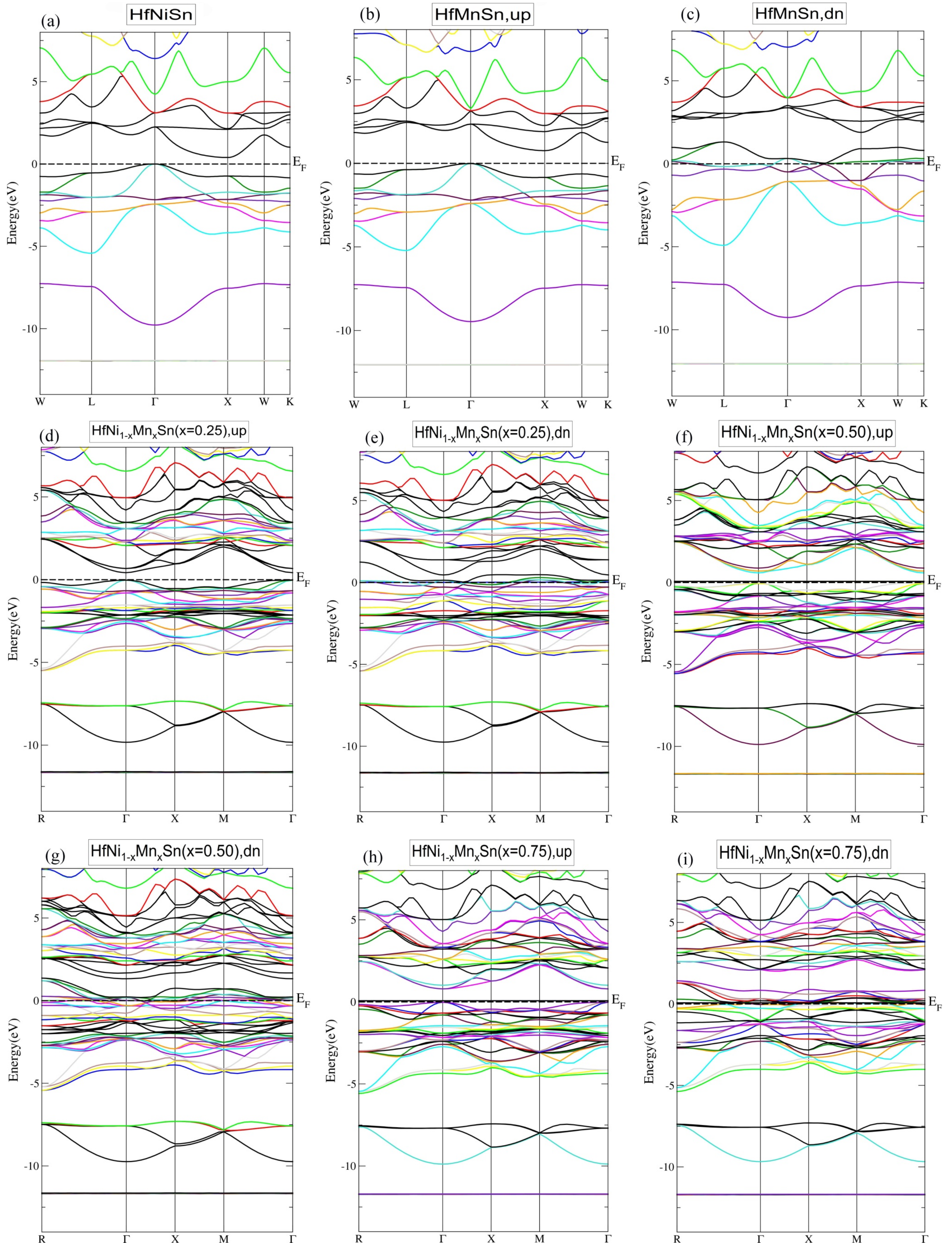

Fig. 5. The bandstructures of (a) HfNiSn, (b-e): HfNiSn, $HfNi_{0.75}Mn_{0.25}Sn$, $HfNi_{0.5}Mn_{0.5}Sn$, $HfNi_{0.25}Mn_{0.75}Sn$ for up spin, and (f-i) HfMnSn, $HfNi_{0.75}Mn_{0.25}Sn$, $HfNi_{0.5}Mn_{0.5}Sn$, and $HfNi_{0.25}Mn_{0.75}Sn$ for dn spin

metal; secondly, in the majority spin, these compounds exhibit semiconductor behavior with a direct gap; and thirdly, the density of states has increased at the Fermi level. At the state of x = 0.25, a direct bandgap of about 0.49eV can be seen in Spin up. On the other hand, the high density of states at the Fermi range for this percentage of substitutions makes this combination a good choice for low-energy optoelectronic and thermoelectric applications. The diagram for x = 0.5 shows that in the spin up, an electron level with a slope of zero is located precisely on the Fermi level, indicating the zero mobility of the holes at this level. In spin down, as the percentage of Mn substitution increases relative to the x = 0.25 state, several electron levels, mostly belonging to 3d-Mn orbitals, shift toward the Fermi level to create a band gap above the Fermi level. In these cases, in spin down, high-gradient levels at the Fermi level have led to these compounds' conductivity. However, in the HfMnSn compound, an indirect gap is observed in the spin up, which increased compared to the HfNiSn. The behavior is still metallic in the spin dn. Moreover, a gap can be seen above the Fermi level and in the conduction region.

3.3. Optical Properties

The optical properties of the HfNiSn compound have been examined under the Mn substitution in Figs. (6a to e). Fig. (6a) shows the behavioral similarity of $\varepsilon_1(\omega)$ for all pure and in presence of Mn substitution in the whole energy range, except for the difference in this function's static value, which has been the

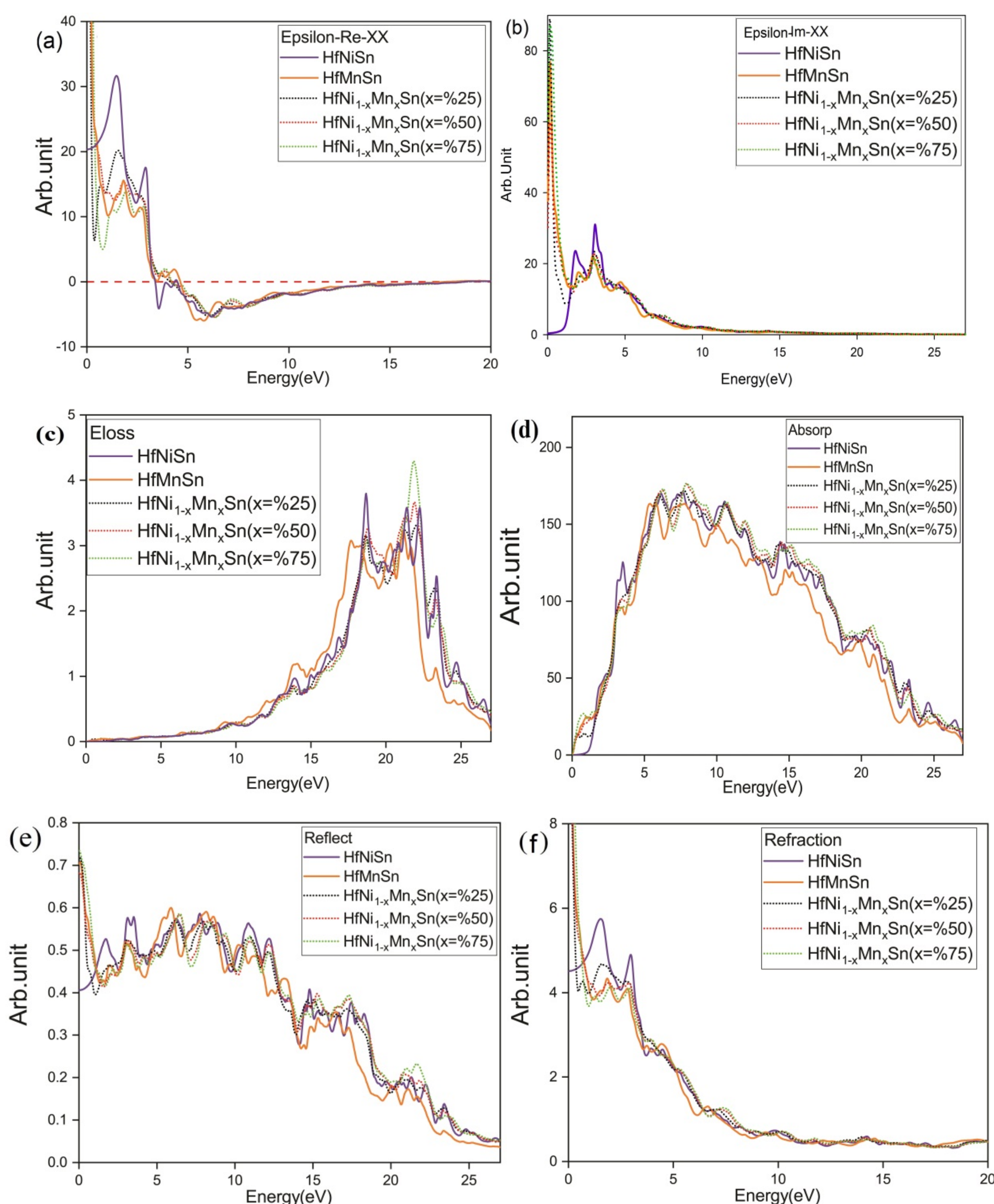

Fig. 6. (a) $\varepsilon_1(\omega)$, (b) $\varepsilon_2(\omega)$, (c) Eloss, (d) Absorption, Reflection, and (Refraction) indexes of HfNiSn in the pure and under Mn substitution cases

constant value of 20 for HfNiSn. Nevertheless, with substitutions, this value has shifted to infinity, representing the metallic behavior of these compounds. In addition to the infrared range, the intensity of the $\varepsilon_1(\omega)$ peaks is common to all states in the visible spectrum, so that they all converge at the ultraviolet edge and show a sharp decrease revealing insulator behavior. Furthermore, most of this function's roots are located in the ultraviolet range, which could be a demonstration of Plasmon frequencies. The oscillating behaviors of these compounds in the infrared and visible range are evidence of small band gaps and their metallic behavior.

Fig. (6b) illustrates the imaginary part of the dielectric function for HfNiSn and under the Mn substitution. As shown, there is a small gap around 1eV for the pure state in the spectrum $\varepsilon_2(\omega)$, displaying the semiconductor behavior of HfNiSn. In the following, two sharp peaks can be detected on the visible and infrared edges, meaning that the electron transitions are due to the light absorption. In contrast to the pure state, in the $HfNi_{1-x}Mn_xSn$ cases, the static value of the imaginary part of the dielectric function tends to infinity, providing the metallic behavior of these compounds and the fact that the electrons are stimulated by the minimal energy gained by light absorption in the infrared region to experience a transition. Interestingly, around the first peak in the pure state, all the substitution states' diagrams have reached a minimum. In the ultraviolet region, all the graphs are convergent since the deeper layers are transferred at these energies, and after 10eV, almost no electrons are transferred. By comparing the refractive index and reflection coefficient, it can be claimed that a significant percentage of the electromagnetic spectrum passes through after 10eV, and this material is transparent.

As shown in Fig. (6c), the common point of all graphs of the energy loss spectrum is that most of the Eloss peaks occurred in the range of 17 to 20eV. The Eloss parameter is referred to the losing optical energy in the matter which may be for various reasons, such as plasmonic oscillations. According to the $\varepsilon_1(\omega)$ roots in this region for all cases, it can be concluded that the peaks of the loss spectrum in this range belong to the Plasmon oscillations and these compounds are generally good candidates for optical and optoelectronic applications in the infrared, visible and ultraviolet regions because they have a high optical response in these areas and their absorption rate is increasing. The Eloss diagrams have zero amounts in the 0eV to 5eV. The HfMnSn Eloss diagram has the red shift than other cases, but it is still a long distance from the visible and UV edge area.

It can be seen from the absorption diagram curves that in the pure state, there is a gap up to about 1eV referring to the semiconductor nature of this compound, but in other cases, the absorption occurs at lower energies due to their metallic nature. Another point is that at the visible edge, the absorption rate rises suddenly to reach its maximum value in the range of 5 to 10eV. Fig. (6e) displays the changes in the reflection coefficient. The static value of this coefficient in pure state is about 0.4, meaning that HfNiSn reflects about 40% of the light, representing a non-metallic behavior. However, in other combinations, the magnitude of static reflection is more significant than 0.7.

Variations in the refractive index are also illustrated in Fig. (6f). The static part of the refractive index for HfNiSn confirms the semiconductor behavior and the highly metallic behavior due to introducing the Mn substitutions. This difference in behavior continues to the visible area, but all combinations show a similar behavior after the ultraviolet edge. The refractive index is less than one at 7eV and afterward. Hence, the group velocity of the electromagnetic wave in this area is greater than the light speed, and these compounds act as a transparent object.

3.4. Electron transport

The temperature-dependent electron transport behavior of HfNiSn under manganese substitutions has been investigated in Fig. 7a to 7e. The trend of Seebeck (S) variations with the presence of Mn is still positive, indicating that this substitution has not had much effect on the semiconductor behavior of this Heusler compound so that HfMnSn has the highest, and $HfNi_{0.75}Mn_{0.25}Sn$ has lower Seebeck than other cases for all temperatures. At room temperature above, their Seebeck amounts are in the 180 to 260 (μVK^{-1}) range, which are comparable to other reported compounds for thermoelectric applications [30,31].

Moreover, electron conductivity changes (σ/τ) also exhibit an increase in the value due to increased vanadium substitution, with HfMnSn receiving the highest conductivity at high temperatures (1200K). In all the combinations, (σ/τ) shows a linear trend by raising the temperature. Power factor, $PF = S^2\sigma/\tau$, also rises by increasing temperature in all cases, and finally, the maximum value of PF at 1200K for the two HfMnSn compounds is about 1.2[$1012 W.m^{-1}.K^{-2}$]. Thermal conductivity of the electron contribution (Kel) can be calculated according to the Wiedemann-Franz law in the form of $L\sigma T = K_{el}$ (where L is the Lorentz number, σ is the electron conductivity and T is the temperature). As shown in Fig. 7d for HfNiSn pure and with Mn substitutions, K_{el} increases with T, with HfNiSn and HfMnSn having the highest values. The calculated figure of merit for the desired combinations is shown in Fig. 7. HfMnSn has the highest ZT value in the entire temperature range (from 100 to 1200K), so that the amount of 0.835 is obtained in the room temperature range for this compound while the maximum ZT for pure HfNiSn is around 0.74 in the room temperature range.

In Boltzmann transport equations, the electrical conductivity is calculated with the σ/τ equation in constant relaxation time (τ) approximation. To calculate the electrical conductivity, it was assumed that the relaxation time σ is independent from the direction, and the relaxation time as a constant at specific temperature and carrier concentration. The reported experimental conductivity for 1% Sb-doped $Zr_{0.5}Hf_{0.5}NiSn_{0.99}Sb_{0.01}$ is 0.855 mΩ cm at 730K, which combined with the calculated σ/τ yields $\tau = 1.21\times10^{-13}$ s for this sample. By using this value into the $= CT^{-1} n^{-1/3}$, the constant amount of $Cn^{-1/3}$ was determined to 8.87×10^{-12} sK, so the relaxation time for HfNiSn was determined to 5.16×10^{-13} s [12].

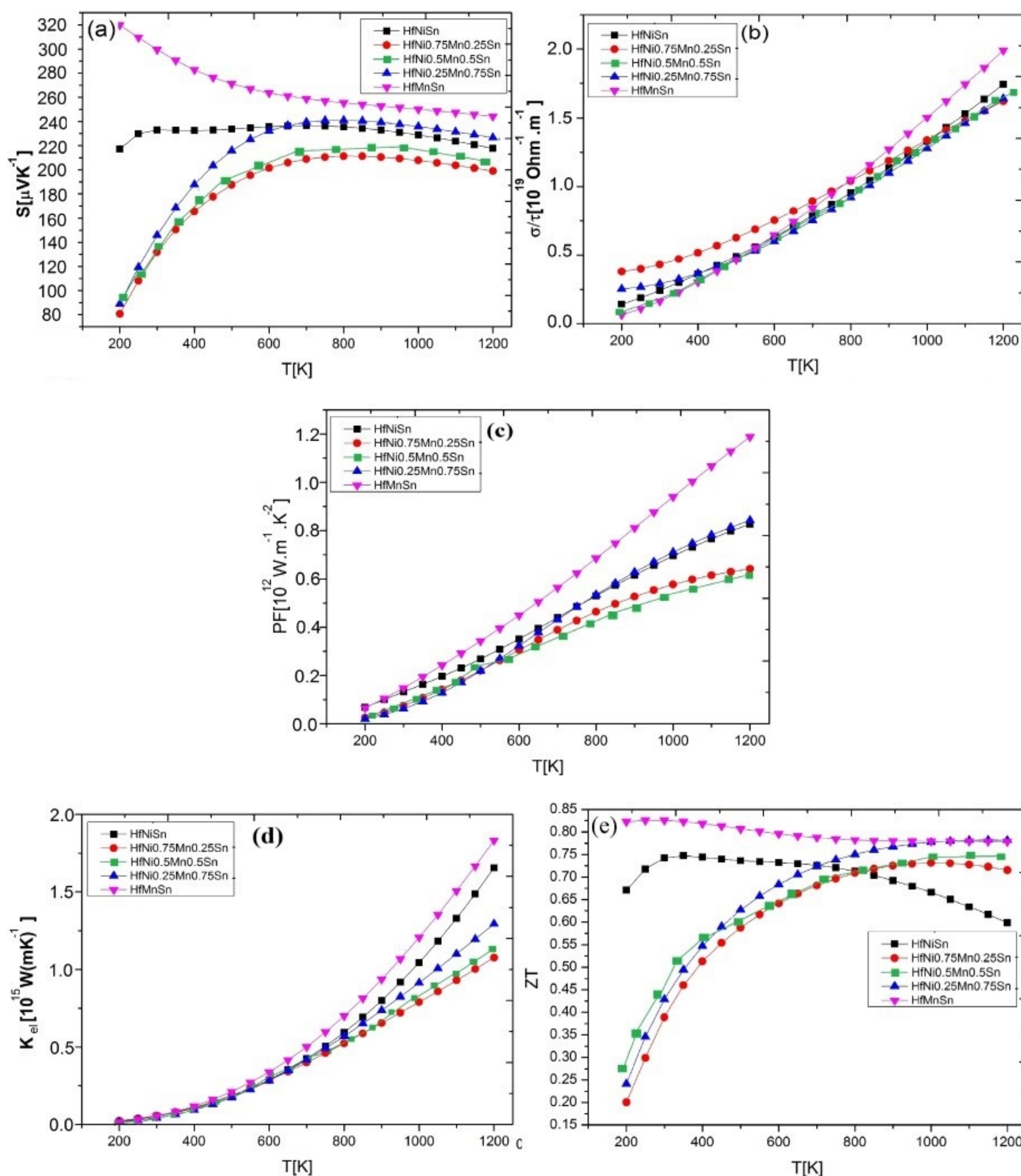

Fig. 7. (a) Seebeck, (b) electrical conductivity, (c) power factor, (d) thermal conductivity, and (e) figure of merit coefficients

4. Conclusion

The mechanical, electronic, optical and thermoelectric properties of the HfNiSn compound in pure state and under Mn substitution were calculated based on density functional theory. Energy-volume calculations showed that all the mentioned compounds have an equilibrium volume and their bulk modulus indicates their relatively high hardness. Compared with other results, the calculated results show that HfNiSn is a non-magnetic semiconductor with a lattice constant close to its experimental value. Electronic calculations with GGA and mBJ approximations showed that the HfNiSn compound is a non-magnetic semiconductor and that the other $HfNi_{1-x}Mn_xSn$ ($x = 0.25, 0.5, 0.75, 1$) compounds are all half-metal with 100% spin polarization at the Fermi level. With increasing percentage of Mn atom substitution, the band gap in the up spin is increased. The HfNiSn and HfMnSn band structures have direct gaps and other $HfNi_{1-x}Mn_xSn$ ($x = 0.25, 0.5, 0.75$) cases have indirect gap compounds.

Optical calculations show that in the range of 0 to 5 eV, all structures have clear optical responses to light emitted and the $\varepsilon_1(\omega)$ sign is positive, but at higher energies, the $\varepsilon_1(\omega)$ sign is negative, indicating an unusual optical behavior. The $\varepsilon_2(\omega)$ curve for HfNiSn has an optical gap that is perfectly consistent with the semiconductor behavior of this compound. At the same time, other compounds do not have a gap and from an optical point of view, they have a metal behavior at low energies. The zeroing of the ELoss spectrum in the infrared, visible, and ultraviolet

regions indicates that these compounds are suitable options for optical applications in these areas. The positive sign of the Seebeck coefficient indicates that the predominant carriers in the carrier transport are holes. At room temperature and above, all compounds are stable in the transport. The power factor curve showed that these compounds are good options for power generators, because increased at higher temperatures. The ZT coefficient in HfNiSn and HfMnSn compounds is relatively constant in all ranges and is around 0.7 and 0.8, which indicates their high thermoelectric quality. Other compounds under the Mn substitution have also reached to the high ZT coefficient.

REFERENCES

[1] S. Populoh, M.H. Aguirre, O.C. Brunko, K. Galazka, Y. Lu, A. Weidenkaff, Scr. Mater. **66** (12), 1073 (2012). DOI: https://doi.org/10.1016/j.scriptamat.2012.03.002
[2] S. Chen, K.C. Lukas, W. Liu, C.P. Opeil, C.P. Chen, Z. Ren, Adv. Energy Mater. **3** (9), 1210 (2013). DOI: https://doi.org/10.1002/aenm.201300336
[3] J. Krez, J. Schmitt, G.J. Snyder, C. Felser, W. Hermes, M. Schwind, J. Mater. Chem. A, **2** (33), 13513 (2014). DOI: https://doi.org/10.1039/C4TA03000A
[4] T. Jaeger, C. Mix, M. Schwall, X. Kozina, J. Barth, B. Balke, G. Jakob, Thin Solid Films, **520** (3), 1010 (2011). DOI: https://doi.org/10.1016/j.tsf.2011.08.008
[5] Y. Kimura, H. Ueno, Y. Mishima, J. Electron. Mater. **38** (7), 934 (2009). DOI: https://doi.org/10.1007/s11664-009-0710-x
[6] C. Yu, T.J. Zhu, R.Z. Shi, Y. Zhang, X.B. Zhao, J. He, Acta Mater. **57** (9), 2757 (2009). DOI: https://doi.org/10.1016/j.actamat.2009.02.026
[7] Q. Shen, L. Chen, T. Goto, T. Hirai, J. Yang, G.P. Meisner, C. Uher, Appl. Phys. Lett. **79**, 4165 (2001). DOI: https://doi.org/10.1063/1.1425459
[8] S. Ouardi, G.H. Fecher, C. Felser, C.G. Blum, D. Bombor, C. Hess, E. Ikenaga, Appl. Phys. Lett. **99** (15), 152112 (2011). DOI: https://doi.org/10.1063/1.3651484
[9] D.P. Rai, A. Shankar, A.P. Sakhya, T.P. Sinha, R. Khenata, M.P. Ghimire, R.K. Thapa, **3**, 075022 (2016). DOI: https://doi.org/10.1088/2053-1591/3/7/075022
[10] D.P. Rai, A. Shankar, Sandeep, M.P. Ghimire, R. Khenata, R.K. Thapa, RSC Adv. **6**, 13358 (2016). DOI: https://doi.org/10.1039/C6RA90008A
[11] K. Ahilan, M.C. Bennett, M.C. Aronson, N.E. Anderson, P.C. Canfield, E. Munoz-Sandoval, J.A., PRB, **69** (24), 245116 (2004). DOI: https://doi.org/10.1103/PhysRevB.69.245116
[12] D.F. Zou, S.H. Xie, Y.Y. Liu, J.G. Lin, J.Y. Li, J. Appl. Phys. **113** (19), 193705 (2013). DOI: https://doi.org/10.1063/1.4804939
[13] H. Hohl, A.P. Ramirez, C. Goldmann, G. Ernst, B. Wölfing, E. Bucher, Journal of Physics: Condensed Matter. **11** (7), 1697 (1999).
[14] N. Shutoh, S. Sakurada, J. Alloys Compd. **389** (1-2), 204 (2005). DOI: https://doi.org/10.1016/j.jallcom.2004.05.078
[15] C. Uher, J. Yang, S. Hu, D.T. Morelli, G.P. Meisner, PRB, **59** (13), 8615 (1999). DOI: https://doi.org/10.1103/PhysRevB.59.8615
[16] B. Arghavani Nia, M. Shahrokhi, R. Moradian, I. Manouchehri, The European Physical Journal – Applied Physics **67** (2) 20403 (2014). DOI: https://doi.org/10.1051/epjap/2014130513
[17] M. Shahrokhi, C. Leonard, Journal of Alloys and Compounds **693**, 1185 (2017). DOI: https://doi.org/10.1016/j.jallcom.2016.10.101
[18] B. ArghavaniNia, M. Shahrokhi, Chinese Journal of Physics 56 (6), 3039 (2018). DOI: https://doi.org/10.1016/j.cjph.2018.10.013
[19] M. Shahrokhi, P. Raybaud, T.L. Bahers, J. Mater. Chem. C, **8**, 9064 (2020). DOI: https://doi.org/10.1039/D0TC02066D
[20] M. Shahrokhi, ACS Omega **5** (2), 1270 (2020). DOI: https://doi.org/10.1021/acsomega.9b03845
[21] K. Schwarz, P. Blaha, G.K.H. Madsen, Comput. Phys. Commun. **147**, 71 (2002). DOI: https://doi.org/10.1016/S0010-4655(02)00206-0
[22] E. Sjöstedt, L. Nordström, D.J. Singh, Solid State Commun. **114**, 15 (2000). DOI: https://doi.org/10.1016/S0038-1098(99)00577-3
[23] G.K.H. Madsen, P. Blaha, K. Schwarz, E. Sjöstedt, L. Nordström, Phys. Rev. B **64**, 195134 (2001). DOI: https://doi.org/10.1103/PhysRevB.64.195134
[24] J.P. Perdew, A. Ruzsinszky, G.I. Csonka, O.A. Vydrov, G.E. Scuseria, L.A. Constantin, X. Zhou, K. Burke, Phys. Rev. Lett. **100**, 136406 (2008). DOI: https://doi.org/10.1103/PhysRevLett.100.136406
[25] H.J. Monkhorst, J. D. Pack, PRB, **13** (12), 5188 (1976). DOI: https://doi.org/10.1103/PhysRevB.13.5188
[26] F.G. Aliev, N.B. Brandt, V.V. Moshchalkov, V.V. Kozyrkov, R.V. Skolozdra, A.I. Belogorokhov, Zeitschrift für Physik B Condensed Matter. **75** (2), 167 (1989). DOI: https://doi.org/10.1007/BF01307996
[27] G.K.H. Madesan, D.J. Sing, Phys. Commun. **175**, 67 (2006). DOI: https://doi.org/10.1016/j.cpc.2006.03.007
[28] F.D. Murnaghan, Proceedings of the national academy of sciences of the United States of America **30** (9), 244 (1944). DOI: https://doi.org/10.1073/pnas.30.9.244
[29] S.H. Wang, H.M. Cheng, R.J. Wu, W.H. Chao, Thin Solid Films **518** (21), 5901 (2010). DOI: https://doi.org/10.1016/j.tsf.2010.05.080
[30] J. Jacob, U. Rehman, K. Mahmood, A. Ali, A. Ashfaq, N. Amin, S. Ikram, M. Alzaid, K. Mehboob, Physics Letters A, **388**, 127034 (2021). DOI: https://doi.org/10.1016/j.physleta.2020.127034
[31] L. Bo, Y. Wang, W. Wang, L. Wang, F. Li, M. Zuo, Y. Ma, D. Zhao, Results in Physics **26**, 104337 (2021). DOI: https://doi.org/10.1016/j.rinp.2021.104337